

**Energy dissipation and defect generation in nanocrystalline silicon carbide**F. Gao,<sup>1,\*</sup> D. Chen,<sup>1,2</sup> Wangyu Hu,<sup>2</sup> and W. J. Weber<sup>1</sup><sup>1</sup>*Pacific Northwest National Laboratory, MS K8-93, P.O. Box 999, Richland, Washington 99352, USA*<sup>2</sup>*Department of Applied Physics, Hunan University, Changsha 410082, China*

(Received 21 September 2009; revised manuscript received 15 February 2010; published 5 May 2010)

Large-scale molecular-dynamics simulations have been employed to study defect generation and primary damage state in nanocrystalline (NC) SiC of average grain diameters from 5 to 21 nm. Primary knock-on atom (PKA) kinetic energies of 10 keV are simulated and cascade structures in NC SiC with a grain size smaller than 12 nm are generally different from those generated in single-crystalline SiC. It is found that the local stresses near the grain boundaries (GBs) strongly affect the behavior of the PKA and secondary recoil atoms (SRAs), and the GBs act as sinks for deposition of kinetic energy. A striking feature is that the PKA and SRAs preferentially deposit energy along the GBs for grains with average size less than 12 nm, which results in atomic displacements primarily within the GBs; whereas for larger grain sizes, most defects are produced within the grains. The defect production within grains generally increases with increasing grain size, which is manifested in switching from grain boundary damage to grain damage. The most common defects created in NC SiC are antisite defects, following by vacancies and interstitials, in contrast to those produced in a single-crystalline SiC, where the dominant defects are Frenkel pairs. Defect production efficiency increases with increasing grain size, with a typical value of 0.18 for small grains and rising to 0.5 for larger grains.

DOI: [10.1103/PhysRevB.81.184101](https://doi.org/10.1103/PhysRevB.81.184101)

PACS number(s): 61.46.Hk, 61.72.Mm, 61.80.Az, 91.60.Ed

**I. INTRODUCTION**

Nanostructured ceramics have opened new and fascinating avenues for research that originates from the observations and expectations of several unique properties of such materials,<sup>1</sup> including very high hardness, high fracture toughness, and superplastic behavior. They also have an increased volume fraction of disordered intergranular regions or grain boundaries, which play a predominant role in the deformation of such materials, as demonstrated in both simulations<sup>2</sup> and experiments.<sup>3</sup> In general, the original microstructure in irradiated materials has substantial effects on the subsequent generation of defects, such as demonstrated with nanocrystalline metals,<sup>4</sup> interfaces of layered composites,<sup>5</sup> and surfaces.<sup>6</sup> These microstructures are believed to be sinks for mobile defects, and interstitial loss to the sinks is considered to be a main driving force for enhanced void swelling under irradiation. Also, nanostructured materials are believed to have substantially different responses to irradiation-induced defects, defect clusters, and amorphization, as compared to the response of single-crystalline materials. In large-grained polycrystalline materials with grain sizes comparable to the characteristic diffusion length of mobile defects, the inter-grain concentrations of accumulated defects and defect clusters are dependent on the rate at which defects and their clusters migrate to and annihilate at grain boundaries. However, it has been argued that extended defect formation should be minimal in grains, if grain sizes are comparable or even smaller than the materials' characteristic defect diffusion length, which is observed as defect-denuded zone width.<sup>7</sup> This is the driving principle behind the concept that radiation tolerance may be enhanced using nanocrystalline materials. The effects of interfaces on defect production in Cu-Ni-layered composites were investigated,<sup>5</sup> and both coherent and semicoherent interfaces were considered. It was interesting to note that defect production and clustering in

the coherent interface, where the relative small stress is uniformly distributed along the interface, are different from those in the semicoherent interface, where there exist localized concentration stresses (an array of misfit dislocations along the interface). Furthermore, the influence of a grain boundary in UO<sub>2</sub> fuel matrix was studied.<sup>8</sup> It was of interest to note that the energy of the cascades is dissipated along the interface and that most of the defects were created at the grain boundary.

Experimentally, Shen *et al.*<sup>7</sup> have demonstrated a substantial enhancement in radiation-induced amorphization resistance for single-phased nanocrystalline (NC) versus large-grained polycrystalline MgGa<sub>2</sub>O<sub>4</sub>. Interstitials migrate much faster than vacancies in this ceramic and can be easily absorbed by the GBs, resulting in a high concentration of vacancies within the grains. The disparities between these defects do not support enhanced radiation tolerance behavior for NC materials. Computer simulations of displacement cascades in NC Ni demonstrated that significant atomic motion toward the surrounding grain boundaries occurs during the thermal spike, with mass transport via a replacement-collision sequence mechanism, which leaves vacancies behind in the grain.<sup>9</sup> The excess vacancies from high energy recoils form a complex partial dislocation network that accommodates in part the reduced atom density within the grain. It is likely that displacement cascades enhance the formation of extended defects, in contrast to the concept of radiation tolerance in NC materials proposed previously.<sup>7</sup> Although several experiments<sup>7,10</sup> have shown that NC structures have increased radiation resistance due to the high density of GBs, the detailed mechanisms causing this enhanced behavior under irradiation are largely unknown.

In this paper, a large-scale molecular dynamics method has been employed to study displacement cascades in NC SiC as a function of grain size, which is a natural step to understand the role of grain boundaries in cascade dynamics and defect generation. The results show that cascade dynam-

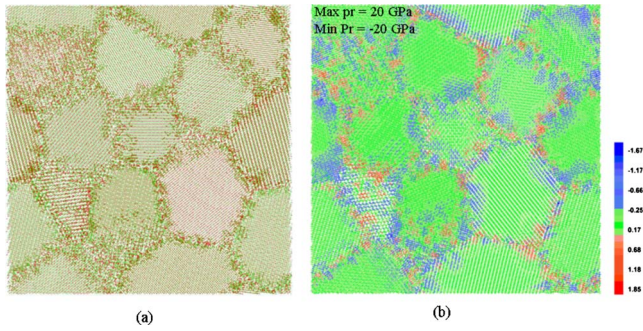


FIG. 1. (Color online) (a) A cross section of nanocrystalline SiC with an averaged grain size of 7.5 nm that exhibits the formation of coexistence of brittle grain and soft amorphous grain boundary phases, where red spheres represent Si atoms and green spheres C atoms, and (b) the local hydrostatic pressure associated each atom, where blue colors indicate the atoms under tensile pressure and red colors under compressive pressure (unit in GPa).

ics, cascade structures, and defect production in small NC SiC are significantly different from those in single-crystalline material. SiC was chosen for this initial study because it represents a well-understood model system for two-component ceramics. There are a large number of investigations on irradiation damage in a single-crystalline and polycrystalline SiC, both experimentally and theoretically, which provide available data for comparison. In addition, SiC is an attractive semiconductor with a wide range of technological applications, such as optoelectronic devices, high-power, high-temperature electronics,<sup>11</sup> and structure components in nuclear reactors.<sup>12</sup> Also, NC SiC films with grain sizes of 5–20 nm have shown “superhardness,” i.e., hardness largely exceeding that of a single-crystalline SiC,<sup>13</sup> which is associated with grain size and the large fraction of amorphous GB phase. In general, solid NC materials are formed with relatively thick amorphous GBs due to the fabrication method.

## II. MODEL AND COMPUTATIONAL APPROACH

The NC-SiC simulation cells are constructed with a widely used Voronoi cell method by distributing grain centers uniformly in a crystalline 3C-SiC, which is believed to contain the essential geometry of NC materials. A set of grains with random orientations is constructed in a simulation box consisting of  $50a_0 \times 50a_0 \times 50a_0$  unit cells ( $1.0 \times 10^6$  atoms) for all the NC-SiC samples, corresponding to 139, 46, 12, 6, and 2 grains with mean grain sizes of 5.2, 7.5, 11.8, 14.9, and 21.5 nm, respectively. The initial atomic configuration is obtained by performing energy optimization to relax any high potential energy configuration that may exist at grain boundaries for a period of 20 ps at 500 K. Three-dimensional periodic boundary conditions are imposed to model a bulk material. The MD simulations are carried out with a constant temperature and constant pressure ensemble with temperature controlled by a N ose-Hoover thermostat<sup>14</sup> and zero pressure with a Parinello-Rahman scheme.<sup>15</sup> The NC SiC is then quenched to 0 K before starting the simulation of a displacement cascade. Figure 1(a) shows the atomic structures of the NC SiC with a grain size of 7.5 nm upon

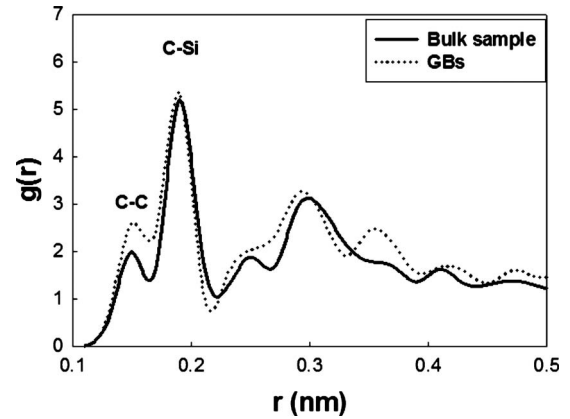


FIG. 2. Mean pair-correlation function,  $g(r)$ , for the grain boundaries in a NC SiC with an averaged grain size of 7.5 nm, together with that calculated in a bulk amorphous sample for comparison. The  $g(r)$  of the GBs is similar to that of the bulk amorphous sample without long-range order and shows liquidlike structures.

annealing at 500 K and it is clear that the nanocrystalline SiC forms with the coexistence of brittle grain and soft amorphous grain boundary phases. In general, the thickness of the grain boundaries is between 1 and 2 nm but somewhat larger disordered regions exist at the triple junctions. To demonstrate these features, the mean total pair-correlation function for the GBs,  $g(r)$ , which quantifies the probability of finding two atoms at an interatomic distance, is calculated and the result is plotted in Fig. 2, together with that for a bulk amorphous sample prepared previously<sup>16</sup> for comparison. The  $g(r)$  of the GBs reveals the typical system without long-range order and liquidlike structure, similar to that of the bulk amorphous SiC. Close inspection of the NC SiC in Fig. 1(a) reveals the presence of highly disordered GBs. Such amorphous grain boundaries are consistent with experimental observations.<sup>17</sup>

The MD simulations of displacement cascades were performed using the MOLDY code, which has been modified to study SiC,<sup>18</sup> with constant volume and periodical boundary conditions. The number of atoms contained in the simulation cell was kept constant while the temperature is controlled by coupling the atoms in the boundary planes to a reservoir of heat at 100 K. A variable-time-step algorithm was employed to allow for a small value early on in the ballistic phase and for a large value when the energy exchange between atoms declined to thermal levels (general from 0.01 to 1 fs). Initially, the MD block was equilibrated for 5 ps at 100 K and then a displacement cascade was initiated by a randomly chosen Si atom in a randomly chosen grain with kinetic energy of 10 keV. The high-index recoil directions of [351] were selected to avoid channeling by primary knock-on atoms (PKAs), and the evolution of the cascade was followed for about 10 ps. For each NC SiC of different grain size, 40 cascades were simulated in order to generate meaningful statistics, which gives the total number of cascades to be 200. Previously, a Wigner-Seitz cell method has been used to identify interstitials, vacancies and antisite defects, which works well for perfect SiC,<sup>19</sup> but may not be suitable to

identify defects in a disordered state, such as amorphous SiC. Thus, a Lindemann sphere method has been employed to identify defects. A vacancy is defined as a site in the undisturbed relaxed lattice which has no atom within a sphere of radius of  $0.22a_0$ , which is half the first nearest distance. An atom is an interstitial if it does not lie within  $0.22a_0$  of a lattice site.

The interactions between atoms were described using Tersoff potentials along with a modification of short-range interactions based on *ab initio* calculations,<sup>20</sup> where the cut-off distances of the potentials were scaled by the cell volume. The threshold displacement energies determined using these potentials are in good agreement with those obtained by first-principles calculations and experimental methods,<sup>21,22</sup> and the melting temperature simulated is in reasonable agreement with the experimental value.<sup>23</sup> These potentials have also been employed to calculate defect properties in 3C-SiC (Ref. 24) and 4H-SiC,<sup>25</sup> and displacement cascades for recoil energies from 0.25 to 50 keV in 3C-SiC.<sup>26</sup> More recently, the same potential was used to study thermal effects in a 10 keV Si PKA cascade in 3C-SiC and the results showed that temperature has small effects on defect generation.<sup>27</sup> These results suggest that the potentials are well suitable for the present simulations of displacement cascade in NC SiC.

In order to understand the effects of grain boundaries on energy dissipation and defect generation, the local pressures within GBs and in grains are calculated. Following a method developed by Cormier *et al.*,<sup>28</sup> the local pressure in a volume of interest,  $\Omega$ , can be defined by

$$P = \frac{1}{3\Omega} \left\langle \sum_i \left( mv_i^2 u_i + \frac{1}{2} \sum_j \vec{F}(r_{ij}) \vec{r}_{ij} b_{ij} \right) \right\rangle, \quad (1)$$

where  $u_i$  is unity if atom  $i$  is within the volume considered and zero otherwise, and  $b_{ij}$  is the fraction of the length of the bond between atom  $i$  and  $j$  within the volume. Equation (1) can be used to accurately calculate the local pressure, and also, satisfies conservation of linear momentum for the chosen volume. In the present study, a sphere centered on each atom, with a radius of 4 Å, has been chosen to calculate the local pressure of this atom, and contains a number of atoms from 19 to 25, which depends on the different regions in the NC SiC.

Also, the amorphous fraction defined as a ratio of amorphous atoms to the total number of atoms, has been calculated. In our previous study of amorphous-to-crystalline transition in 4H-SiC,<sup>29</sup> a procedure to identify crystalline and amorphous atoms was established. The NC SiC with different sizes was equilibrated at 100 K, and the coordination number and the three-body correlation function were averaged over several hundred simulation time steps. Then, these functions are compared with those in a perfect crystal which are also calculated by averaging the atomic positions for the same time at the same temperature to identify crystalline and amorphous atoms. The time for averaging atomic positions is about three picoseconds, which is enough to get accurate averaged configurations to discriminate between crystalline and amorphous atoms. If a Si or a C atom is fourfold coordinated with its neighbors (C or Si atoms) and the six pos-

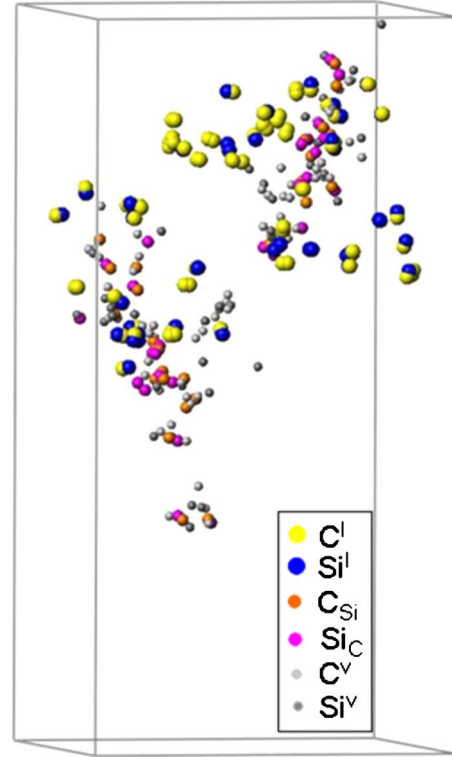


FIG. 3. (Color online) Defect distribution produced by a 10 keV cascade at the final damage state in a single crystalline 3C-SiC. The defect type is distinguished by size and grayscale.

sible angles between the corresponding bonds fall within the limits of the averaged distribution for a perfect crystal at the same temperature, the atom is considered to be crystalline. Conversely, if this condition is not fulfilled, the atom is denoted as part of an amorphous network.

### III. RESULTS AND DISCUSSIONS

#### A. General comments on defect generation in bulk SiC

Previously, a number of computational studies have been performed to investigate the displacement threshold energies and single-displacement cascades for energies up to 50 keV in SiC using variations in the Tersoff potentials.<sup>20,23,26,30</sup> These studies have provided important insights into the mechanisms that control defect production in displacement cascades and also statistics on the number of arrangement of the defects generated as a function of energy. Self-atom recoils in SiC generate multiple branches along the path, resulting in the formation of distinct regions separated each other and a highly dispersed cascade, which is independent of PKA energy. Figure 3 shows the final defect distribution of a 10 keV cascade in 3C-SiC, from which it is clearly seen that the defects are spread over the simulation cell. Most surviving defects are single interstitials and vacancies, with a small fraction of defects in clusters. It has been observed that the size of defect clusters is small, particularly for vacancy clusters, and defect clusters containing more than four defects are rare within a single 10 keV cascade.<sup>26</sup> The nature of cascade geometry in SiC may be due to its high melting

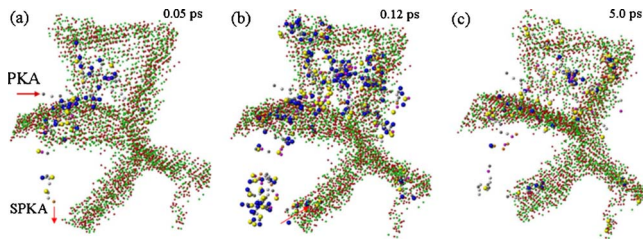


FIG. 4. (Color online) Computer plots showing defect generation processes in a NC SiC with an averaged grain size of 7.5 nm at (a) 0.05 ps, (b) 0.12 ps, and (c) 5.0 ps, where the defect type is distinguished by size and gray. The Si PKA generates multiple secondary recoils, and they preferentially travel along the GBs, resulting in the most damage distributed along the GBs.

temperature, light masses, and small scattering cross sections for Si and C atoms, which inhibits the formation of a highly densified cascade and the development of a thermal-spike phase. The cascade lifetime in SiC is very short, resulting in the poor atomic mixing. These features, together with high migration energies of most defects, provide a physical basis for cascade formation and defect generation in SiC, which is in significant contrast to the features observed in metals and alloys.<sup>31,32</sup>

### B. Cascade formation in NC SiC

As described above, a large number of displacement cascades have been simulated in single-crystalline SiC and the physical mechanisms for cascade formation are well understood so that a full assessment of cascade formation in NC SiC can be made in terms of grain size. Figure 4 shows three stages of a 10 keV Si cascade in a NC SiC with a mean grain size of 7.5 nm, where only defects and the atoms in GBs are presented. The interstitials are represented by large spheres, vacancies by small gray ones and antisite defects by middle-sized spheres, as shown in the legend in Fig. 3. The 10 keV Si was started in the grain, as indicated by an arrow in Fig. 4(a), and there is a rapid build up in the number of displaced atoms during collisional process until a maximum in the number is reached in about 0.12 ps. It is noted that the PKA moves toward a nearby GB and initiates a number of secondary recoil atoms (SRAs) in the GB. A striking feature is that these SRAs preferentially travel along the GBs, and generate multiple regions of displaced atoms, as shown in Fig. 4(b), resulting in most displaced atoms along the GBs, rather than in the grains. However, one of the secondary recoils penetrates through the GB, and generates a number of displacements in one of the grains, as shown at the left bottom corner of Fig. 4(b). There are several possible reasons for the observed phenomena. The GBs consist of amorphous structures, and the atomic density is generally lower than that in the grains, which may provide easy channels for recoil atoms to travel. In general, the GBs are made of adjacent regions of high compression and tension compared to the pressure in the grain interior. The local hydrostatic pressure in a section of the NC SiC sample with a mean grain size of 7.5 nm is shown in Fig. 1(b), where the thickness of the section is  $4a_0$  ( $a_0$  is the lattice constant of 3C-SiC). Some of

the GBs have a compressive side toward one grain and a tensile side toward the other grain while the triple junctions consist of larger compressive and tensile regions (up to 20 and  $-20$  GPa). The local pressure in the grain interior shows a uniform distribution and the variation in the pressure is very small. As long as the PKA moves into the GB, the PKA generates a number of the SRAs, as described above. These SRAs interact with the local stresses surrounding the GBs and their movements are strongly affected by the local stresses along the GBs. For instance, one of the SRAs at the left bottom corner of Fig. 4(a) initially moves along the direction indicated by an arrow, but it suddenly changes its direction, when it falls into the stress region of the GB, and preferentially travels along the GB, as shown by an arrow in Fig. 4(b). It is of interest to note that the GBs act as sinks for the PKA or SRAs to deposit their kinetic energies. The total number of vacancies and interstitials produced in the grains for this cascade are 21 and 3, respectively, the sum of which is much smaller than those generated in a single-crystalline SiC. Previous cascade simulations at grain boundaries in bcc iron<sup>4</sup> demonstrated that most replacement collisional cascades do not permeate through the boundary and the boundary generally acts as a region where defects build up. Approximately 70–90 % defects produced lie inside the grain boundary regions, which depends on the type of the grain boundaries. In the coherent model of Cu-Ni layered composites,<sup>5</sup> defect production is generally similar to that in bulk materials, and the defects are distributed at the interfaces and in the Cu or Ni layer, which suggests that small uniform stress has negligible effects on defect generation. In the semicoherent model, it was also observed that the PKA deposits most of its energy into the interface, similar to that observed in the coherent model. A striking feature of the cascade damage near the semicoherent interface is the formation of stacking faultlike defects associated with the misfit dislocations (Lomer-Cottrell dislocations). In the Ni layer, the triangular-shaped defect cluster attached to the misfit dislocation is a stacking fault pyramid of vacancies, while the interstitial clusters are observed at the misfits in the Cu layer, forming pyramidal structures. These results demonstrated that local stresses strongly affect the PKA behavior and cascade formation. In the study of a grain boundary in  $\text{UO}_2$  fuel matrix,<sup>8</sup> it was observed that the cascade does not penetrate through the GB, but the atoms are displaced instead along the grain boundary, with most energy dissipating along the interface. Although there is no a comprehensive theory to fully describe the interaction of the PKA or SRAs with highly concentrated stresses, the present results have illustrated that the low atomic density and high local stresses at the GBs (see Fig. 1) strongly affect the behavior of the PKA and SRAs, particularly when the size of the GBs is comparable with the cascade size. The strong interaction between the PKA or SRAs and the GBs leads them to preferentially travel and dissipate their kinetic energies along the GBs.

Figure 5 shows the defect generation of a 10 keV cascade in NC SiC, with the grain size of 21 nm, where only defects and the atoms in the GBs are presented. Similar to the case of 7.5 nm SiC, a Si atom at the middle of the grain is chosen to start a displacement cascade, with a recoil direction along the  $[351]$ , and the PKA moves toward one of the grain

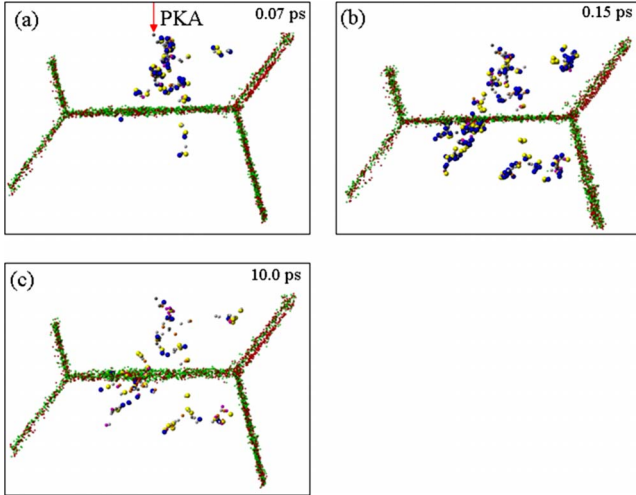


FIG. 5. (Color online) Computer plots showing defect generation processes in a NC SiC with an averaged grain size of 21.5 nm at (a) 0.07 ps, (b) 0.15 ps, and (c) 10.0 ps, where the defect type is distinguished by size and grayscale. The cascade structure is similar to that created in a single-crystalline SiC and defects are generated on both sides of the grain boundary.

boundaries. In general, the defect generation is similar to that in a single-crystalline SiC, i.e., the PKA creates multiple branches and forms a dispersed cascade. In this case, the size of the grains is much larger than the cascade size, and the interfaces form flat planes, such that the effect on the PKA behavior is very small. However, it is observed that the PKA deposits some of its kinetic energy into the GB, resulting in rearrangement of existing atoms or creating defects at the GB, as seen in Fig. 5(c), but the influence of the GB on cascade formation is small. Also, it can be seen that the PKA penetrates through the GB and creates defects on both sides of the GB. Most defects generated are single interstitials and vacancies, and the total number of defects produced within the grains is about 46 for the case shown in Fig. 5 (It is difficult to define a defect at the GB because of amorphous structure), as compared with the averaged value of 69 for 10 keV cascades in a single crystalline SiC. It is of interest to note that the maximum travel distance of the PKA averaged

over all the cascades considered in the NC SiC (21.5 nm) is about 9.9 nm, which is smaller than the averaged value of 17.4 nm in a single-crystalline SiC (based on the previous cascade data). It appears that the GB acts as a hard wall for a PKA to penetrate, and thus, reduces the maximum travel distance. The present simulations clearly illustrate that defect production within the grains strongly depends on the grain size, and there is a transition from grain damage to GB damage.

### C. Defect production

The final number of defects produced in a cascade is an important parameter for theory and up-scale model of defect evolution with microstructures. The previous simulations<sup>26</sup> showed that the number of defects produced in single-crystalline SiC is generally less than that predicted by the standard Norgett, Robinson, and Torrens (NRT) formula,<sup>33</sup> and the efficiency of defect production is about 0.4 as compared to the NRT prediction. Thus, it is of interest to compare the defect production in the NC SiC with that in a single-crystalline SiC and the estimation from NRT formula that is given by

$$N_{\text{NRT}} = \frac{0.8E_{\text{PKA}}}{2\bar{E}_d}, \quad (2)$$

where  $E_{\text{PKA}}$  is the damage energy in the MD simulation and  $\bar{E}_d$  is the averaged value of threshold displacement energy. As indicated in Ref. 34 the application of Eq. (2) to a multicomponent compound is not straightforward because each element (or sublattice) in the compound has different threshold energies and antisite defects can also be produced. Here, the weighted average  $E_d$  is used and taken to be 22 eV, as suggested by the computer simulations in SiC,<sup>34</sup> which is close to experimental observations. The calculated  $N_{\text{NRT}}$  value is about 182 for a 10 keV cascade.

The final number of defects created within the grains of NC SiC is shown in Fig. 6(a) as a function of grain size, where the interstitials, vacancies, and antisite defects are presented separately, and the bars represent the standard error. The number of defects produced within the grains generally

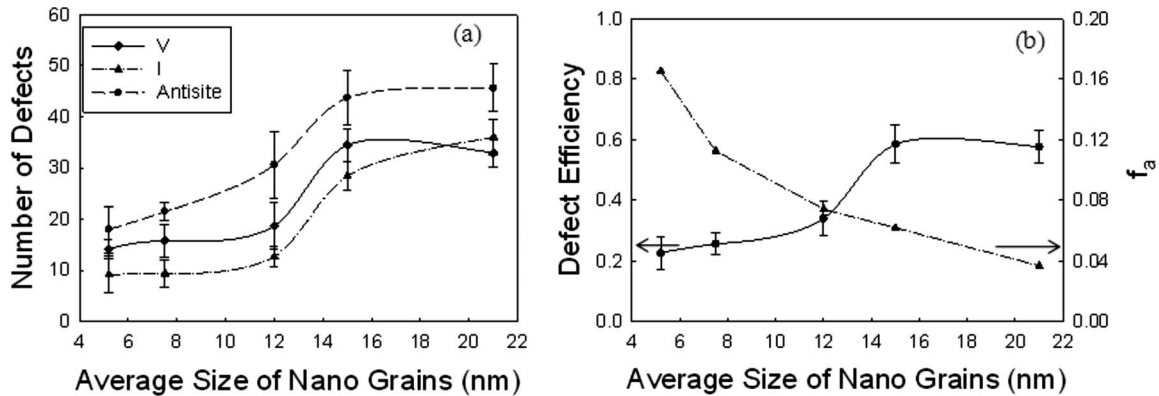


FIG. 6. (a) Final number of defects produced, averaged over all the displacement cascades considered, as a function of grain size, and (b) the efficiency of defect production, as defined by Eq. (2), and amorphous fraction,  $f_a$ . Both increase with increasing grain size and show defect production by a competition between grain boundary damage and grain damage.

increases with increasing grain size. The numbers of defects are small when the grain size is less than 12 nm, which suggests that most displacements are associated with the GBs, whereas the numbers of defects become larger when the grain size is larger than 12 nm. It may be a transition in defect production, which is manifested in switching from grain boundary dominant damage (the rearrangements of the atoms in amorphous boundaries) to grain dominant damage (similar to bulk damage of SiC). The C vacancies outnumber the Si vacancies by a factor of about 3.2; the C interstitials also outnumber the Si interstitials by a factor of about 2.4. This ratio varies slightly with increasing grain size. The most common defects created within grains in NC SiC are antisite defects, followed by vacancies and interstitials, in contrast to those produced in single-crystalline SiC where the dominated defects are Frenkel pairs, rather than antisites.<sup>26</sup> This is due to the fact that most antisite defects are directly generated by long and short replacements along the paths of PKA and secondary PKAs during the collisional phase before the maximum displacements are reached, and thermally induced antisite defects within a cascade in SiC are few.<sup>26</sup> The weak thermal-spike and high migration energies of antisite defects in SiC inhibit the recovery of antisite defects, surviving within cascade volume. However, it should be noted that the number of antisite defects in bulk SiC is much larger than that in NC SiC for the same recoil energy. Similar to the damage in single-crystalline SiC, the number and size of both interstitial and vacancy clusters are very small for all the grain sizes considered. The efficiency of defect production, defined as a ratio of the total defects generated to the NRT value, is shown in Fig. 6(b) as a function of grain size, where the bars indicate the standard error. Also, the amorphous fraction as a function of grain size,  $f_a$ , is imposed for comparison. The efficiency increases rapidly with increasing grain size, from 0.23 for the small grains to 0.55 for the larger grains. The value of 0.55 is in good agreement with that obtained for 10 keV cascades in single crystalline SiC. The amorphous fraction generally decreases with increasing grain size, which is consistent with the trend of defect production efficiency within the grains, and the observed behavior is correlated with a competition between grain boundary damage and grain damage. To further demonstrate this, the DD ratio of defects produced within the grains to total number of displacements (defined as atoms that are displaced from their original sites within  $0.22a_0$  distance), is calculated, and the results are shown in Fig. 7 as a function of the grain size. The DD ratio is correlated with the energy dissipation of the PKAs and SRAs along the grain boundaries, and provides a criterion for energy partition between the grain boundaries and grains. All the defects created have a similar behavior; the DD ratio increases with increasing the grain size, which is in agreement with the grain size dependence of damage behavior observed above. It is clear that the energy dissipation is mainly along the GBs when the grain size is smaller than 12 nm and decreases rapidly with increasing the grain size.

#### D. Discussion

In general, defect generation in polycrystalline SiC and the corresponding mechanisms strongly depend on grain

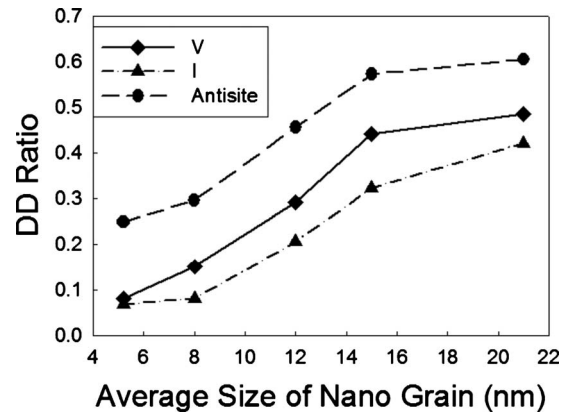


FIG. 7. DD ratio, defined as defects produced within the grains to atoms that are displaced from their original sites within  $0.22a_0$  distance, as a function of the grain size, showing an increase with increasing the grain size.

size, and the interactions of the PKAs or SRAs with the local stresses near grain boundaries affect their movements. It has been observed that these SRAs preferentially travel along the GBs when the grain size is smaller than 12 nm, resulting in the production of most damage in the GBs. There exists a transition in the defect generation from grain damage to grain boundary damage. This is mainly due to the interaction probability of the PKAs or SRAs with grain boundaries and the observed damage behavior occurs during the collisional phase. Recent MD simulations of cascades in nanocrystalline Ni (Ref. 9) reveal that the self-interstitial atoms (SIAs) and their clusters created within displacement cascades can be attracted by the GBs, and significant atomic motion toward the surrounding GBs occurs during the thermal spike phase. Also, the local stress strongly affects the motion of SIAs and their clustering, and even large SIA clusters can undergo a change in direction, leading to one- or two-dimensional motion, which gives rise to the difference in the primary damage state between NC and single crystalline Ni. However, significant movement of SIAs in SiC is not observed during the thermal-spike phase, even if they are close the GBs where the variation in local stress is large, in contrast to those observed in NC metals. The relative high migration energies of defects<sup>35</sup> and weak thermal spike<sup>26</sup> in SiC may account for these different phenomena. It is likely that the probability for the recoil atoms to preferentially travel along the GBs controls the primary damage structure in NC SiC. The number of defects produced within the grains in NC SiC is generally less than that in single-crystalline SiC for the same PKA energy considered. On average, about 75.8–60 % fewer defects are produced, when the GB size is smaller than 12 nm, than in single-crystalline SiC, and only about 27% less when the GB size is larger than 12 nm. These results suggest that the small grain size decreases the number of defect produced within the grains and the PKA deposits most of its energy into the grain boundaries. However, the detailed analysis of the grain boundaries (highly disordered regions) reveals that the significant amorphization does not occur along the GBs during the cascade process, and most of the deposited energy leads to the rearrangement of atoms within the GBs without increasing the thickness of the GBs. It is not

yet clear if the specific features of defect generation in NC SiC can result in a substantial enhancement in radiation-induced amorphization resistance, or affect the subsequent behavior of the material. The complete understanding of this issue needs the further study of defect accumulation in NC SiC, as demonstrated by our previous simulation in single crystalline SiC.<sup>19</sup>

Experimentally, several physical mechanisms have been suggested to explain some of the differences in radiation damage behavior between various small and large-grained materials.<sup>7,10</sup> The thermodynamic considerations proposed two effects on irradiated polycrystalline materials, i.e., the increase in the system free energy as grain size is reduced and free energy changes associated with irradiation. Also, if defects annihilate preferentially at interfaces, the system free energy must necessarily rise faster with increasing irradiation dose in large-grained material. The combination of these effects implies that systems with smaller grain size are not necessarily more radiation tolerant. There are other thermodynamic considerations that are associated with disparities between the mobilities of interstitials and vacancies produced under an irradiation environment. It is generally believed that vacancies are far less mobile than interstitials, particularly at low temperatures, and thus, they cannot easily reach these interfaces as readily as freely migrating interstitials, resulting in a number of surviving vacancies within the grains. As such, vacancy concentrations should be larger in NC materials, as compared to large-grained materials, because fewer mobile interstitials are available within the grains of NC materials to annihilate immobile vacancies. However, this idea is unlikely to explain the enhanced radiation tolerance behavior of NC materials. The present studies clearly demonstrate a different mechanism of defect production in NC SiC, which is associated with the local stress gradients in the vicinity of the GBs and low atomic density at the GBs, such that the PKA and SRAs are strongly trapped at the GBs when the size of GBs is comparable with the cascade size. In this case, most of the damage in the small NC SiC is along the GBs, rather than within the grains. It has been observed that the number of vacancies within the grains is slightly larger than that of the interstitials for NC SiC with GB sizes less than 12 nm but the difference is small. For example, the total vacancies produced in the NC SiC with a grain size of 12 nm, averaged over all the cascades considered, are about 18.7, as compared to about 12.5 interstitials created within the grains. The vacancy concentration within GBs in SiC is low. This behavior is significantly different from that observed in metals, where large vacancy concentrations are present within the grains, because most of the interstitials produced are thermally absorbed by the GBs dur-

ing the thermal spike phase, but not vacancies.<sup>9</sup> These excess vacancies are dominant defects within the grains and form complex partial dislocation networks. As defect accumulation are considered, all these mechanisms described above may have the potential to either enhance or diminish the radiation tolerance of NC versus large-grained ceramics but it is not clear to what extent. These issues need to be further examined in future experimental and theoretical studies.

#### IV. SUMMARY

The NC SiC with grain sizes ranging from 5.2 to 21 nm has been prepared using a molecular-dynamics method, and the calculated pair-correlation function demonstrated that NC SiC forms with a coexistence of brittle grain and soft amorphous grain boundary phases. These NC materials have been employed to study the effects of grain boundaries on cascade structures and defect production with PKA energy of 10 keV. The results show that the cascade structures in the NC SiC with grain size smaller than 12 nm are considerably different from those observed in a single-crystalline SiC, which may be due to the fact that the local stresses near the GBs strongly affect the behavior of the PKA and SRAs, resulting in them preferentially traveling along the GBs. It is of interest to note that most damage is along the GBs in the NC SiC with small grain size, while the most damage forms within the grains for larger grain size. Defect generation, production efficiency, and DD ratio all suggest defect production by a competition between GB damage and grain damage. These features are significantly different from those observed in metals, where a large number of vacancies are present within grains.

Antisite defects are the most common defects in NC SiC, following by vacancies and interstitials, where the dominated defects are Frenkel pairs in a single-crystalline SiC. Defect production efficiency within grains increases with increasing grain size, ranging from 0.18 in the NC SiC with small grain size to 0.5 for larger grains. The mechanism of defect production observed in NC SiC sheds light on the competition between different damage underlying design and tailoring NC ceramics for radiation-induced amorphization resistance.

#### ACKNOWLEDGMENTS

This research is supported by the Division of Materials Sciences and Engineering, Office of Basic Energy Sciences, U.S. Department of Energy under Contract No. DE-AC05-76RL01830. D. Chen and W. Y. Hu were supported by Chinese Academy of Sciences and the National Natural Science Foundation under Contract No. 50671035. D.C. also wishes to acknowledge the China Scholarship Council.

\*Corresponding author. FAX: 1-509 371 6242; fei.gao@pnl.gov

<sup>1</sup>R. W. Siegel, in *Nanomaterials: Synthesis, Properties and Applications*, edited by A. S. Edelstein and R. C. Cammarata (Institute of Physics, Bristol, 1996), pp. 201–218.

<sup>2</sup>J. Schiotz, T. Vegge, F. D. Di Tolla, and K. W. Jacobsen, *Phys.*

*Rev. B* **60**, 11971 (1999).

<sup>3</sup>D. Chen, X. F. Zhang, and R. O. Ritchie, *J. Am. Ceram. Soc.* **83**, 2079 (2000).

<sup>4</sup>M. Samaras, P. M. Derlet, H. Van Swygenhoven, and M. Victoria, *Phys. Rev. B* **68**, 224111 (2003).

- <sup>5</sup>H. L. Heinisch, F. Gao, and R. J. Kurtz, *J. Nucl. Mater.* **329-333**, 924 (2004).
- <sup>6</sup>S. G. Mayr and R. S. Averback, *Phys. Rev. B* **68**, 214105 (2003).
- <sup>7</sup>T. D. Shen, S. Feng, M. Tang, J. A. Valdez, Y. Wang, and K. E. Sickafus, *Appl. Phys. Lett.* **90**, 263115 (2007).
- <sup>8</sup>L. V. Brutzel and J. P. Crocombette, in *Structure and Refractory Materials for Fusion and Fission Technologies*, edited by J. Aktaa, M. Samaras, M. Serrano de Caro, M. Victoria, and B. Wirth, MRS Symposia Proceedings No. 981E (Materials Research Society, Pittsburgh, 2007), p. 0981.
- <sup>9</sup>M. Samaras, P. M. Derlet, H. Van Swygenhoven, and M. Victoria, *Phys. Rev. Lett.* **88**, 125505 (2002).
- <sup>10</sup>M. Rose, A. G. Balogh, and H. Hahn, *Nucl. Instrum. Methods Phys. Res. B* **127-128**, 119 (1997).
- <sup>11</sup>P. Melinon, B. Masenelli, F. Tournus, and A. Perez, *Nature Mater.* **6**, 479 (2007).
- <sup>12</sup>K. Minato, K. Sawa, K. Koya, T. Tomita, A. Ishikawa, C. A. Baldwin, W. A. Gabbard, and C. M. Malone, *Nucl. Technol.* **131**, 36 (2000).
- <sup>13</sup>F. Liao, S. L. Girshick, W. M. Mook, W. W. Gerberich, and M. R. Zachariah, *Appl. Phys. Lett.* **86**, 171913 (2005).
- <sup>14</sup>S. Nóse, *J. Phys.: Condens. Matter* **2**, SA115 (1990).
- <sup>15</sup>M. Parrinello and A. Rahman, *J. Appl. Phys.* **52**, 7182 (1981).
- <sup>16</sup>F. Gao and W. J. Weber, *J. Appl. Phys.* **89**, 4275 (2001).
- <sup>17</sup>X. F. Zhang, M. E. Sixta, and L. C. De Jonghe, *J. Am. Ceram. Soc.* **83**, 2813 (2000).
- <sup>18</sup>F. Gao, W. J. Weber, and W. Jiang, *Phys. Rev. B* **63**, 214106 (2001).
- <sup>19</sup>F. Gao and W. J. Weber, *Phys. Rev. B* **66**, 024106 (2002).
- <sup>20</sup>R. Devanathan, W. J. Weber, and T. Diaz de la Rubia, *Nucl. Instrum. Methods Phys. Res. B* **141**, 118 (1998).
- <sup>21</sup>R. Devanathan and W. J. Weber, *J. Nucl. Mater.* **278**, 258 (2000).
- <sup>22</sup>F. Gao, H. Y. Xiao, X. T. Zu, M. Posselt, and W. J. Weber, *Phys. Rev. Lett.* **103**, 027405 (2009).
- <sup>23</sup>F. Gao and W. J. Weber, *Phys. Rev. B* **63**, 054101 (2000).
- <sup>24</sup>F. Gao, E. J. Bylaska, W. J. Weber, and L. R. Corrales, *Phys. Rev. B* **64**, 245208 (2001).
- <sup>25</sup>M. Posselt, F. Gao, W. J. Weber, and V. Belko, *J. Phys.: Condens. Matter* **16**, 1307 (2004).
- <sup>26</sup>F. Gao, W. J. Weber, and R. Devanathan, *Nucl. Instrum. Methods Phys. Res. B* **180**, 176 (2001).
- <sup>27</sup>D. E. Farrell, N. Berntein, and W. K. Liu, *J. Nucl. Mater.* **385**, 572 (2009).
- <sup>28</sup>D. J. Cormier, J. M. Rickman, and T. J. Delph, *J. Appl. Phys.* **89**, 99 (2001).
- <sup>29</sup>F. Gao, Y. Zhang, M. Posselt, and W. J. Weber, *Phys. Rev. B* **74**, 104108 (2006).
- <sup>30</sup>L. Malerba and J. M. Perlado, *Phys. Rev. B* **65**, 045202 (2002).
- <sup>31</sup>D. J. Bacon, F. Gao, and Yu. N. Osetsky, *J. Nucl. Mater.* **276**, 1 (2000).
- <sup>32</sup>D. A. Terentyev, L. Malerba, R. Chakarova, K. Nordlund, P. Olsson, M. Rieth, and J. Wallenius, *J. Nucl. Mater.* **349**, 119 (2006).
- <sup>33</sup>M. J. Norgett, M. T. Robinson, and I. M. Torrens, *Nucl. Eng. Des.* **33**, 50 (1975).
- <sup>34</sup>R. Devanathan, W. J. Weber, and F. Gao, *J. Appl. Phys.* **90**, 2303 (2001).
- <sup>35</sup>F. Gao, W. J. Weber, M. Posselt, and V. Belko, *Phys. Rev. B* **69**, 245205 (2004).